Quark chiral condensate from the overlap quark propagator [*]

Chao Wang(王超)[1,2;1]   Yujiang Bi(毕玉江)[3]   Hao Cai(蔡浩)[3],

Ying Chen(陈莹)[1,2]   Ming Gong(宫明)[1,2]   Zhaofeng Liu(刘朝峰)[1,2;2]

[1]Institute of High Energy Physics and Theoretical Physics Center for Science Facilities,
Chinese Academy of Sciences, Beijing 100049, China
[2]School of Physics, University of Chinese Academy of Sciences, Beijing 100049, China
[3]School of Physics and Technology, Wuhan University, Wuhan 430072, China

Abstract: From the overlap lattice quark propagator calculated in the Landau gauge, we determine the quark chiral condensate by fitting operator product expansion formulas to the lattice data. The quark propagators are computed on domain wall fermion configurations generated by the RBC-UKQCD Collaborations with $N_{\rm f} = 2+1$ flavors. Three ensembles with different light sea quark masses are used at one lattice spacing $1/a = 1.75(4)$ GeV. We obtain $\langle \bar{\psi}\psi \rangle^{\overline{\rm MS}}(2 \text{ GeV}) = (-304(15)(20) \text{ MeV})^3$ in the $SU(2)$ chiral limit.

1   Introduction

The strong interactions among quarks and gluons have two prominent features at low energies: confinement and chiral symmetry breaking. The quark chiral condensate $\langle \bar{\psi}\psi \rangle$, in the light quark massless limit, is the order parameter of the spontaneous chiral symmetry breaking in Quantum Chromodynamics (QCD), the theory describing the strong interaction. Furthermore $\Sigma \equiv -\langle \bar{\psi}\psi \rangle$ is one of the two low energy constants of chiral perturbation theory, the low energy effective theory of QCD, at leading order. The quark chiral condensate also appears in QCD sum rules and is an important input parameter.

Thus there have been many determinations of the chiral condensate from different ways by using lattice QCD, which is a nonperturbative method to solve QCD from first principles. See, for examples, Refs [1–9]. A review of the evaluations of the chiral condensate on the lattice can be found in Ref. [10].

In this work, we determine the $SU(2)$ low energy constant Σ by comparing the Operator Product Expansion (OPE) of the quark propagator in momentum space in the continuum $\overline{\rm MS}$ scheme with the lattice calculation of the propagator in Landau gauge. This strategy was used by the ETM Collaboration in a calculation with two flavors of dynamical Wilson twisted mass fermions [11]. Our analysis is based on 2+1-flavor domain wall fermion configurations and overlap valence quarks. There have also been analyses using staggered fermions [12], the OPE of the pseudoscalar vertex [13, 14] and the OPE of the quark propagator in coordinate space [15].

Our final result, obtained at one lattice spacing, is $\Sigma^{1/3} = 304(15)(20)$ MeV in the $\overline{\rm MS}$ scheme at the renormalization scale 2 GeV. Here the first error contains uncertainties from statistics, the lattice spacing and truncation effects in perturbative calculations. The second error is an estimate of the $\mathcal{O}(a^2 g^2)$ lattice artifacts in our data.

In the rest of the paper, we first discuss the OPE of the quark propagator in the $\overline{\rm MS}$ scheme in Section 2. Then our lattice setup is given in Section 3. The analyses of the quark propagator and the results of the chiral condensate are presented in Section 4. Finally we summarize in Section 5.

2   OPE of the quark propagator

For a quark field ψ with mass $m_{\rm q}$, its propagator in momentum space $S_q(p)$ can be written as

$$S_q(p) \equiv \int \mathrm{d}^4 x e^{-\mathrm{i}p \cdot x} \langle T\psi(x)\bar{\psi}(0)\rangle = \frac{-\mathrm{i}\not{p}V(p^2)}{p^2} + \frac{S(p^2)}{p^2}, \quad (1)$$

where the dressing functions $S(p^2)$ and $V(p^2)$ will be called the scalar and vector form factor respectively at below. The OPE of these two form factors renormalized in the $\overline{\mathrm{MS}}$ scheme in Landau gauge was calculated to three loops in Ref. [16]. Up to operators of dimension three, one has

$$S_R(p^2) = S_{PT}(\mu, p^2)m_{\mathrm{q}}(\mu) + \frac{C_{m^3}(\mu, p^2)}{p^2}m_{\mathrm{q}}^3$$

$$+ \frac{C_{mA^2}(\mu, p^2)}{p^2}\langle m_{\mathrm{q}}A^2\rangle$$

$$+ \frac{C_{\bar{\psi}\psi}(\mu, p^2)}{p^2}\langle\bar{\psi}\psi\rangle(\mu), \quad (2)$$

and

$$V_R(p^2) = V_{PT} + \frac{C_{m^2}(\mu, p^2)}{p^2}m_{\mathrm{q}}^2 + \frac{C_{A^2}(\mu, p^2)}{p^2}\langle A^2\rangle. \quad (3)$$

Here the purely perturbative parts S_{PT} and V_{PT} were computed at three loops in Ref. [17]. The Wilson coefficients C_{m^3}, C_{mA^2}, $C_{\bar{\psi}\psi}$, C_{m^2} and C_{A^2} at three loops can be found in Ref. [16].

In principle, if we can obtain the scalar and vector form factors by lattice QCD, then we can fit the lattice data to the functions in Eqs. (2, 3) to extract out the quark mass and the chiral condensate. Since we need the inverse powers of p^2 to suppress the contributions from higher dimension operators, the lower limit of the fitting range in p^2 cannot be too small. The Wilson coefficients are calculated by perturbation theory. This also requires that p^2 cannot be too small. On the other hand, if p^2 is too large then $\mathcal{O}(a^2p^2)$ and higher order lattice discretization effects in the data will be out of control. Thus one needs to find a fitting window in which a stable and reliable value for the chiral condensate can be obtained.

Before the fittings we do not know if such a window exists or not given the lattice spacing in our data. Therefore we will vary our fitting range to test the reliability of our results. We shall take the lattice discretization artifacts into account in our error analysis.

3   Lattice setup

We use the 2+1-flavor domain wall fermion configurations generated by the RBC-UKQCD Collabora-

tions [18]. The parameters of the ensembles used in this analysis are given in Table 1.

Table 1.   Parameters of the 2+1-flavor domain wall fermion configurations generated by the RBC-UKQCD Collaboration. The lattice spacing was determined in Ref. [19].

$1/a$/GeV	label	$am_l^{\mathrm{sea}}/am_s^{\mathrm{sea}}$	volume	N_{conf}
1.75(4)	c005	0.005/0.04	$24^3 \times 64$	92
	c01	0.01/0.04	$24^3 \times 64$	88
	c02	0.02/0.04	$24^3 \times 64$	138

Three light sea quark masses are used to check the sea quark mass dependence of our results.

We use overlap fermions for the valence quark. The massless overlap operator [20] is defined as

$$D_{ov}(\rho) = 1 + \gamma_5 \varepsilon(\gamma_5 D_{\mathrm{w}}(\rho)). \quad (4)$$

Here ε is the matrix sign function and $D_{\mathrm{w}}(\rho)$ is the usual Wilson fermion operator, except with a negative mass parameter $-\rho = 1/2\kappa - 4$ in which $\kappa_c < \kappa < 0.25$. In our calculation we use $\kappa = 0.2$ which corresponds to $\rho = 1.5$. The massive overlap Dirac operator is defined as

$$D_m = \rho D_{ov}(\rho) + m\left(1 - \frac{D_{ov}(\rho)}{2}\right)$$

$$= \rho + \frac{m}{2} + \left(\rho - \frac{m}{2}\right)\gamma_5\varepsilon(\gamma_5 D_{\mathrm{w}}(\rho)). \quad (5)$$

To accommodate the $SU(3)$ chiral transformation, it is usually convenient to use the chirally regulated field $\hat{\psi} = \left(1 - \frac{1}{2}D_{ov}\right)\psi$ in lieu of ψ in the interpolation field and operators. That is to say, our valence quark propagator is

$$G \equiv D_{\mathrm{eff}}^{-1} \equiv \left(1 - \frac{D_{ov}}{2}\right)D_m^{-1} = \frac{1}{D_c + m}, \quad (6)$$

where $D_c = \frac{\rho D_{ov}}{1 - D_{ov}/2}$ is chiral, i.e. $\{\gamma_5, D_c\} = 0$ [21].

The overlap valence quark masses in lattice units are given in Table 2. The corresponding pion masses range from 220 to 600 MeV.

Table 2.   The overlap valence quark masses am_q in lattice units used in this analysis.

0.00620	0.00809	0.01020	0.01350	0.01720	0.02430	0.03650	0.04890

Our quark propagators are calculated by using a point source on each configuration. The numbers of configurations used in this work are given in Table 1. For three of the valence quark masses (0.01350, 0.02430, 0.04890) on ensemble c005, eight point sources on each configuration are used. For the same three quark masses on ensemble c02, eight point sources are used on half of the 138 configurations. The eight point sources are evenly distributed on the time slices and randomly distributed in 3-space from configuration to configuration to reduce autocorrelations. Part of these propagators were calculated and used in the computation of renormalization constants [22] and in the study of diquarks [23]. We average the quark propagators from the eight sources on each configuration for these three valence quark masses. Then together with the data from other configurations for other quark masses a Jackknife procedure (one configuration eliminated each time) is done to get the statistical uncertainties in our analyses below. Since ensemble c01 has the least statistics, the result from it will have the largest uncertainty, while c005 will have the smallest statistical uncertainty.

Anti-periodic and periodic boundary conditions are used respectively in the time and spatial directions. Therefore the momentum modes are

$$ap = \left(\frac{2\pi k_1}{L}, \frac{2\pi k_2}{L}, \frac{2\pi k_3}{L}, \frac{(2k_4+1)\pi}{T} \right), \qquad (7)$$

where $k_\mu = -6, -5, \cdots, 6$. To reduce Lorentz noninvariant discretization effects, we use the momentum modes close to the diagonal line. This is achieved by doing a cut as was done in Ref. [22]

$$\frac{p^{[4]}}{(p^2)^2} < 0.32, \quad \text{where } p^{[n]} = \sum_{\mu=1}^{4} p_\mu^n, \quad p^2 = \sum_\mu p_\mu^2. \quad (8)$$

4   Analysis and discussion

From Eq. (1) we have

$$\frac{1}{12}\text{Tr}[S_q(p)] = \frac{S(p^2)}{p^2}, \qquad \frac{1}{12}\text{Tr}[i\not{p}S_q(p)] = V(p^2). \quad (9)$$

In Fig. 1 we show the bare scalar and vector form factors ($S(p^2)/p^2$ and $V(p^2)$) in lattice units from our data ensemble c02 as functions of a^2p^2.
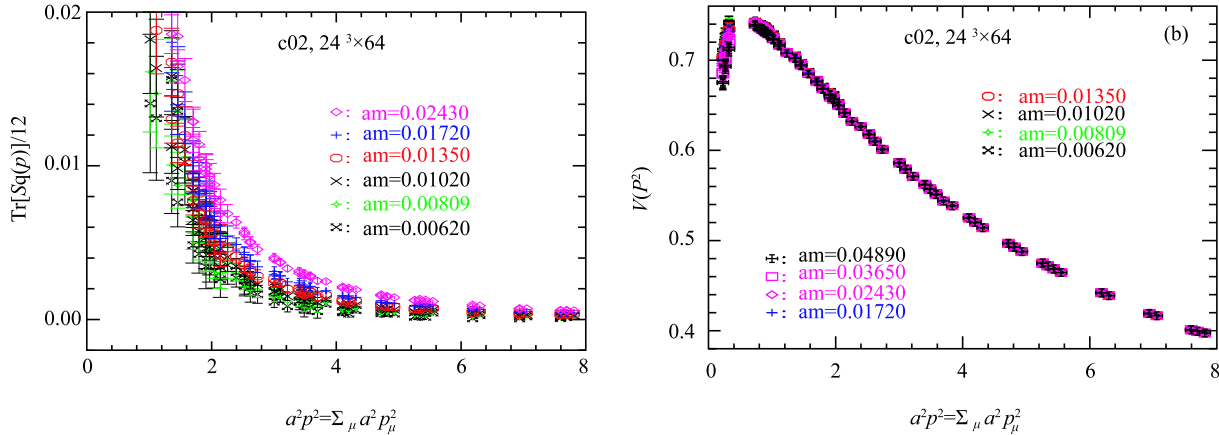

Fig. 1.   (color online) (a) The bare scalar form factor $S(p^2)$ divided by a^2p^2 from the quark propagators for various valence quark masses. (b) The bare vector form factor $V(p^2)$ for various valence quark masses.

The scalar form factor has a visible quark mass dependence, as is shown in the graph on the left. The vector form factor, however, in the graph on the right, has no visible quark mass dependence even in the quite low p^2 region. For example, at $a^2p^2 = 1.114$ the vector form factors for $am_q = 0.00620$ and 0.04890 agree with each other within the statistical uncertainties (0.720(4) versus 0.717(3)). This indicates that the contribution from the m_q^2 term is quite small in Eq. (3). Therefore we can also expect that the m_q^3 term in Eq. (2) is negligible. Indeed, below we will see that the quark mass dependence of the scalar form factor can be well described by a linear function.

In our analyses below we take into account the reduced $\mathcal{O}(a^2p^2)$ discretization effects by adding a term proportional to a^2p^2 in the fitting functions. However there are other artifacts of $\mathcal{O}(a^2g^2)$. In Ref. [11] the authors find that $\mathcal{O}(a^2g^2)$ effects are substantial in the vector form factor V, but modest in the ratio S/V. Since we have not computed the lattice artifacts of $\mathcal{O}(a^2g^2)$ and thus cannot remove them from our form factors, we estimate their effects in our results by comparing the chiral condensates obtained from analyzing the ratio of the form factors and from analyzing the scalar form factor

alone. The difference in the results from the two analyses will be taken as a systematic uncertainty.

4.1   Analysis of the ratio of scalar to vector form factor

Since the ratio is expected to have much smaller $\mathcal{O}(a^2 g^2)$ lattice artifacts than the scalar form factor, we trust more on the chiral condensate from the analysis of the ratio. The number from this analysis will be taken as our final result.

The gluon condensate $\langle A^2 \rangle$ in Landau gauge was determined in, for example, Refs. [24, 25]. In the analysis of Ref. [11], a compatible value of $\langle A^2 \rangle$ was found but it did not seem to be stable yet against the order in perturbation theory. Since $\langle A^2 \rangle / p^2 < \sim 0.6 \text{ GeV}^2/4 \text{ GeV}^2 = 0.15$ is small in the range of p^2 in our following analysis and the corresponding Wilson coefficient $|C_{A^2}|$ is also small (~ 0.3), we ignore the contribution from this condensate in Eq. (3) as a first step (note V_{PT} is of order 1). To obtain information about $\langle A^2 \rangle$ from analyzing the vector form factor, we need more statistics and need to subtract the $\mathcal{O}(a^2 g^2)$ artifacts.

The quark mass dependence of the vector form factor is quite small, as was seen in Fig. 1. This indicates that we can keep only the first term on the right-hand side of Eq. (3) in analyzing our data. Thus from Eqs. (2,3), we

have for the bare and renormalized form factors

$$\frac{S_0}{V_0} = \frac{S_R}{V_R} = \frac{S_{PT}}{V_{PT}} m(\mu) + \frac{C_{\bar{\psi}\psi}(\mu, p^2)}{p^2 V_{PT}} \langle \bar{\psi}\psi \rangle. \qquad (10)$$

Here the quark field renormalization constants Z_q in the numerator and denominator cancel each other.

Defining a ratio

$$R \equiv \frac{\text{Tr}[S_q(p)]}{\text{Tr}[i\not{p} S_q(p)]} = \frac{S(p^2)}{p^2 V(p^2)}, \qquad (11)$$

then in the chiral limit we have

$$\lim_{m_q \to 0} R = \frac{C_{\bar{\psi}\psi}(\mu, p^2)}{(p^2)^2 V_{PT}} \langle \bar{\psi}\psi \rangle. \qquad (12)$$

In lattice units and taking into account $\mathcal{O}(a^2 p^2)$ lattice artifacts in the quark propagator, we use the following function

$$\lim_{m_q \to 0} \frac{R}{a} = \frac{C_{\bar{\psi}\psi}(\mu, p^2)}{(a^2 p^2)^2 V_{PT}} a^3 \langle \bar{\psi}\psi \rangle + B a^2 p^2. \qquad (13)$$

to fit the ratio obtained from our lattice quark propagator. The dimensionless quark chiral condensate $a^3 \langle \bar{\psi}\psi \rangle$ and B are two fit parameters.

In the graph on the left of Fig. 2 we show the ratio R (in lattice units) as a function of $a^2 p^2$ from ensemble c02 for various valence quark masses.
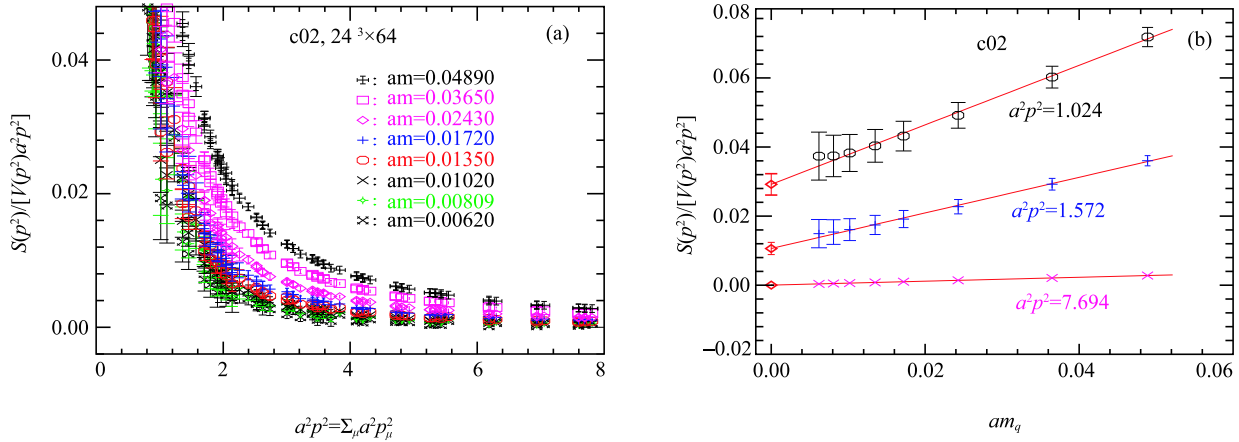

Fig. 2.   (color online) (a) The ratio of form factors for various valence quark masses. (b) Examples of linear extrapolation to the quark massless limit at three typical momentum values.

The graph on the right of Fig. 2 shows examples of the linear chiral extrapolation of R at three typical momentum values: $a^2 p^2 = 1.024$, 1.572 and 7.694. At all momentum values in our data for R we see a good linear dependence on am_q.

Then we fit the ratio R in the chiral limit to the func-

tion Eq. (13). Figure 3 shows an example of the fitting using a fitting range $a^2 p^2 \in [2.2, 5.3]$. The fitting in the right-hand graph does not include the $B a^2 p^2$ term. Comparing it with the fitting in the left-hand graph, which does contain this term, we see that the $B a^2 p^2$ term decreases the χ^2/dof significantly.
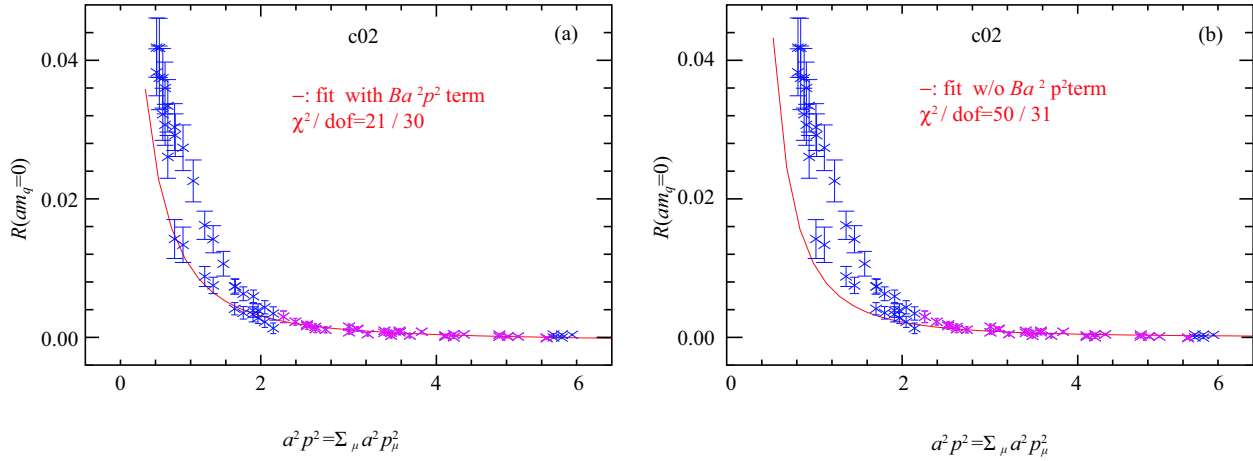
Fig. 3.   (color online) (a) Fitting of the ratio R in the valence quark massless limit. (b) The same fit as in the left graph but without the Ba^2p^2 term. The data points in purple ($a^2p^2 \in [2.2, 5.3]$) are included in the fittings.

In evaluating the Wilson coefficients in the fitting function, we use $\Lambda_{\mathrm{QCD}}^{\overline{\mathrm{MS}}} = 332(17)$ MeV for three flavors in the $\overline{\mathrm{MS}}$ scheme [26] to compute the strong coupling constant α_s. $\alpha_s^{\overline{\mathrm{MS}}}(2$ GeV$)$ is calculated by using its perturbative running to 3-loops, since the Wilson coefficients are only known to 3-loops. From this fitting, we get $\langle\bar{\psi}\psi\rangle^{\overline{\mathrm{MS}}}(2$ GeV$) = -(303(36)(7)$ MeV$)^3$ by using the lattice spacing $1/a = 1.75(4)$ GeV [19]. Here the first uncertainty is statistical and the second is from the uncertainty in the lattice spacing.

To check the stability of the result against the fitting range, we vary the lower and upper limits of a^2p^2. In Table 3, we give the $\chi^2/$dof of the fittings and the results of $\langle\bar{\psi}\psi\rangle$ against these changes. As we see from the table, we can get a stable value for $\langle\bar{\psi}\psi\rangle$.

Table 3. $\langle\bar{\psi}\psi\rangle^{\overline{\mathrm{MS}}}(2$ GeV$)$ from fittings of R with different fitting ranges on ensemble c02. The first uncertainty is statistical and the second is from the uncertainty in the lattice spacing.

$a^2p^2 \in$	$p^2 \in$/GeV^2	$\chi^2/$dof	$(\langle\bar{\psi}\psi\rangle)^{1/3}$/MeV
$[2.2, 5.5]$	$[6.7, 16.8]$	0.89	$-296(36)(7)$
$[2.2, 5.3]$	$[6.7, 16.2]$	0.71	$-303(36)(7)$
$[2.2, 5.1]$	$[6.7, 15.6]$	0.74	$-301(36)(7)$
$[2.2, 4.9]$	$[6.7, 15.0]$	0.76	$-301(37)(7)$
$[2.2, 4.7]$	$[6.7, 14.4]$	0.79	$-305(38)(7)$
$[2.6, 5.3]$	$[8.0, 16.2]$	0.67	$-294(41)(7)$
$[2.4, 5.3]$	$[7.4, 16.2]$	0.63	$-297(39)(7)$
$[2.0, 5.3]$	$[6.1, 16.2]$	0.83	$-305(35)(7)$
$[1.8, 5.3]$	$[5.5, 16.2]$	1.09	$-314(31)(7)$

We then check the truncation error from the perturbative expansion of the Wilson coefficients. We repeat the fittings with Wilson coefficients and α_s being evalu-

ated at 2-loops and 1-loop. The resulted numbers from data ensemble c02 are collected in Table 4.

Table 4. $\langle\bar{\psi}\psi\rangle^{\overline{\mathrm{MS}}}(2$ GeV$)$ from fittings of R on ensemble c02 with different truncation order (n-loops) in evaluating the Wilson coefficients and α_s. The fitting range is $a^2p^2 \in [2.2, 5.3]$.

n	$\chi^2/$dof	$(\langle\bar{\psi}\psi\rangle)^{1/3}$/MeV
1	0.73	$-323(39)(8)$
2	0.72	$-312(37)(7)$
3	0.71	$-303(36)(7)$

Taking the difference between the center values with $n = 2$ and $n = 3$ as a systematic error, we finally get $\langle\bar{\psi}\psi\rangle^{\overline{\mathrm{MS}}}(2$ GeV$) = (-303(36)(7)(9)$ MeV$)^3$ on ensemble c02. This is collected in Table 7.

Similarly, in Table 5 and Table 6 we give the results from various fitting ranges on the other two ensembles c01 and c005 respectively. The truncation effects in the Wilson coefficients and α_s are examined too. The quark condensates from all three ensembles are listed in Table 7.

Table 5. $\langle\bar{\psi}\psi\rangle^{\overline{\mathrm{MS}}}(2$ GeV$)$ from various fitting ranges on ensemble c01. The first uncertainty is statistical and the second is from the uncertainty in the lattice spacing.

$a^2p^2 \in$	$p^2 \in$/GeV^2	$\chi^2/$dof	$(\langle\bar{\psi}\psi\rangle)^{1/3}$/MeV
$[1.8, 3.8]$	$[5.5, 11.6]$	1.01	$-296(39)(7)$
$[1.8, 3.6]$	$[5.5, 11.0]$	1.05	$-297(40)(7)$
$[1.8, 3.4]$	$[5.5, 10.4]$	1.13	$-291(42)(7)$
$[2.2, 3.8]$	$[6.7, 11.6]$	0.87	$-299(50)(7)$
$[2.0, 3.8]$	$[6.1, 11.6]$	0.77	$-291(45)(7)$
$[1.6, 3.8]$	$[4.9, 11.6]$	1.31	$-318(29)(7)$

Table 6. $\langle\bar{\psi}\psi\rangle^{\overline{\mathrm{MS}}}$(2 GeV) from various fitting ranges on ensemble c005. The first uncertainty is statistical and the second is from the uncertainty in the lattice spacing.

$a^2p^2 \in$	$p^2 \in/\mathrm{GeV}^2$	χ^2/dof	$(\langle\bar{\psi}\psi\rangle)^{1/3}/\mathrm{MeV}$
$[1.4, 3.3]$	$[4.3, 10.1]$	1.16	$-302(11)(7)$
$[1.4, 3.1]$	$[4.3, 9.5]$	0.92	$-306(11)(7)$
$[1.4, 2.9]$	$[4.3, 8.9]$	0.99	$-306(11)(7)$
$[1.8, 3.1]$	$[5.5, 9.5]$	0.80	$-302(16)(7)$
$[1.6, 3.1]$	$[4.9, 9.5]$	0.73	$-299(13)(7)$
$[1.2, 3.1]$	$[3.7, 9.5]$	0.95	$-309(10)(7)$

Table 7. $\langle\bar{\psi}\psi\rangle^{\overline{\mathrm{MS}}}$(2 GeV) on the three ensembles. The first uncertainty is statistical. The second is from the uncertainty of the lattice spacing. The third is an estimate of the truncation effects in the evaluations of the Wilson coefficients and α_s.

ensemble	$a^2p^2 \in$	$p^2 \in/\mathrm{GeV}^2$	χ^2/dof	$(\langle\bar{\psi}\psi\rangle)^{1/3}/\mathrm{MeV}$
c02	$[2.2, 5.3]$	$[6.7, 16.2]$	0.71	$-303(36)(7)(9)$
c01	$[1.8, 3.8]$	$[5.5, 11.6]$	1.01	$-296(39)(7)(11)$
c005	$[1.4, 3.1]$	$[4.3, 9.5]$	0.92	$-306(11)(7)(13)$

We also tried to do fittings in the same momentum range $a^2p^2 \in [2.0, 3.2]$ on all three ensembles. What we found is given in Table 8.

Table 8. $\langle\bar{\psi}\psi\rangle^{\overline{\mathrm{MS}}}$(2 GeV) from the same fitting window $a^2p^2 \in [2.0, 3.2]$ on all three ensembles. The three uncertainties are as explained in Table 7.

ensemble	χ^2/dof	$(\langle\bar{\psi}\psi\rangle)^{1/3}/\mathrm{MeV}$
c02	0.97	$-322(39)(8)(12)$
c01	0.83	$-278(53)(6)(10)$
c005	0.85	$-303(18)(7)(12)$

Besides all the above, we repeated the fittings with $\langle A^2\rangle^{\overline{\mathrm{MS}}}$(2 GeV) fixed to 0.6 GeV^2 in Eq. (3). The resulting changes in $(\langle\bar{\psi}\psi\rangle)^{1/3}$ are 3 to 4 MeV, much smaller than the statistical or other uncertainties. This means that it is safe to ignore the contribution from $\langle A^2\rangle$ with our current statistics.

The light sea quark mass dependence is shown in Fig. 4, where we plot together the results from all three ensembles. The three red octagons are those in Table 7 from fittings with a different p^2 range on each ensemble. The blue diamonds are those in Table 8 from fittings in the same momentum range on all three ensembles. In this graph, we have quadratically combined together the three uncertainties in Table 7 and Table 8 respectively. Since we do not see an apparent sea quark mass dependence with our relatively large uncertainties, we do a

constant fit to finally obtain

$$\langle\bar{\psi}\psi\rangle^{\overline{\mathrm{MS}}}(2 \text{ GeV}) = (-304(15) \text{ MeV})^3$$
$$\text{(different fitting ranges)}, \tag{14}$$

and

$$\langle\bar{\psi}\psi\rangle^{\overline{\mathrm{MS}}}(2 \text{ GeV}) = (-304(19) \text{ MeV})^3$$
$$\text{(same fitting range)}. \tag{15}$$
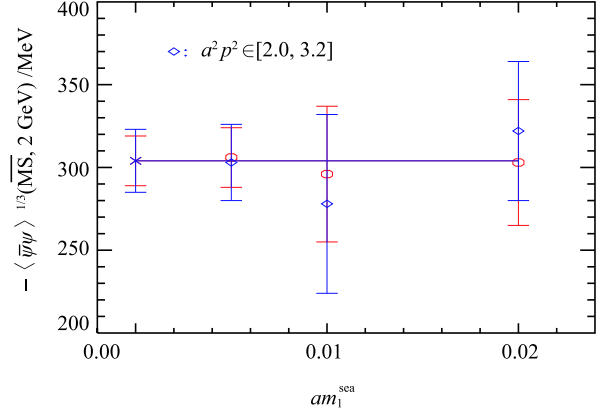
These two numbers are in good agreement with each other.

Fig. 4.   (color online) The light sea quark mass dependence of $\langle\bar{\psi}\psi\rangle^{\overline{\mathrm{MS}}}$(2 GeV). The crosses are from constant fits.

4.2   Analysis of the Scalar form factor

There may be non-negligible $\mathcal{O}(a^2g^2)$ lattice artifact in our scalar and vector form factors, as were seen in Ref. [11] with Wilson twisted mass fermions. At large p^2, difference was seen in the $\mathcal{O}(a^2g^2)$-corrected and uncorrected vector form factor [11]. Unfortunately, we have not calculated this artifact yet and therefore could not do this correction to our data. To estimate its effects, we analyze the scalar form factor in the chiral limit to obtain the chiral condensate and compare the result with the one from Section 4.1.

From Eq. (2) we see that in the chiral limit the scalar form factor is related to the chiral condensate by

$$S_R(p^2) = \frac{C_{\bar{\psi}\psi}(\mu, p^2)}{p^2}\langle\bar{\psi}\psi\rangle(\mu). \tag{16}$$

With a quark field renormalization constant $\psi_R = Z_q^{1/2}\psi$ and taking into account $\mathcal{O}(a^2p^2)$ effects, we have

$$\frac{1}{12}\mathrm{Tr}[S_q(a,p)] = \frac{S_0(a^2p^2)}{a^2p^2} = \frac{S_R(a^2p^2)}{Z_q a^2p^2}$$

$$= \frac{C_{\bar{\psi}\psi}(\mu, p^2)}{Z_q(a^2p^2)^2}a^3\langle\bar{\psi}\psi\rangle(\mu) + Ba^2p^2. \tag{17}$$

Here we have put everything in lattice units. Thus the quark field renormalization constant Z_q is needed in the analysis of the scalar form factor.

4.2.1 Quark field renormalization

Our Z_q is first calculated in the RI-MOM scheme [27] and then converted to the $\overline{\text{MS}}$ scheme. The detailed calculation in the RI-MOM scheme for our work can be found in Ref. [22]. We first use the axial vector Ward Identity to obtain Z_A^{WI}, which equals Z_A in the RI-MOM scheme. Then, from it, Z_q in the RI-MOM scheme is computed at several valence quark masses. The results for Z_q show little quark mass dependence (see Fig. 3 in Ref. [22]). We now do a linear extrapolation of Z_q in the quark mass to the chiral limit. The results in this limit for data ensemble c005 are shown by the black diamonds in Fig. 5.
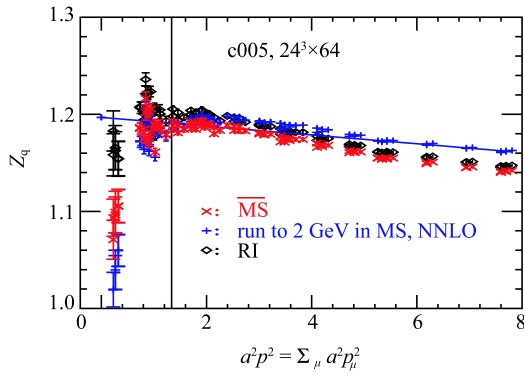

Fig. 5.   (color online) The quark field renormalization constant for ensemble c005. The black vertical line indicates the position of $\mu = 2$ GeV.

Then the conversion ratio calculated by perturbation theory [17] to 3 loops is used to get Z_q in the $\overline{\text{MS}}$ scheme, which is shown by the red crosses in Fig. 5. After running $Z_q^{\overline{\text{MS}}}$ from an initial scale p^2 to $\mu^2 = (2 \text{ GeV})^2$ by using its anomalous dimension to 3-loops, we obtain the blue

pluses in Fig. 5. The deviation of the blue pluses from a constant at large initial scales is attributed to $\mathcal{O}(a^2 p^2)$ lattice artifacts. Thus a linear extrapolation in $a^2 p^2$ to $a^2 p^2 = 0$ is done to get $Z_q^{\overline{\text{MS}}}(2 \text{ GeV})$ (illustrated by the blue line using data points at $a^2 p^2 > 5$).

The results of Z_q in the $\overline{\text{MS}}$ scheme are given in Table 9 for all three ensembles.

Table 9. $Z_q^{\overline{\text{MS}}}(2 \text{ GeV})$ on the three ensembles. The first error is statistical and the second is a 1% systematic error.

ensemble	c02	c01	c005
$Z_q^{\overline{\text{MS}}}/(2 \text{ GeV})$	1.202(2)(12)	1.209(3)(12)	1.197(2)(12)

Similarly to what has been done to Z_S for the scalar density in Ref. [22] (see its Tab. V), we find a 1% systematic uncertainty for Z_q from the uncertainty in the lattice spacing, the uncertainty in $\Lambda_{\text{QCD}}^{\overline{\text{MS}}}$, the truncation error of the perturbative conversion ratio and the variation of the fitting range in the $a^2 p^2$ linear extrapolation. This systematic uncertainty is given in Table 9.

4.2.2 Fitting results

We have shown the scalar form factor (divided by p^2) in the left-hand graph of Fig. 1. In Fig. 6 we show the linear chiral extrapolation of the scalar form factor and the fitting of the chiral limit results to the function Eq. (17).

Again, we find in the fit that the $B a^2 p^2$ term decreases χ^2/dof significantly. As was done in the analysis of the ratio of form factors in Section 4.1, we check the stability of the results of $\langle \bar{\psi}\psi \rangle$ against the fitting range in p^2, and against the order of truncation in the evaluations of the Wilson coefficients and α_s. Since the uncertainty of Z_q is quite small compared with other sources of uncertainties, we have ignored its propagation to the uncertainty of the quark chiral condensate.
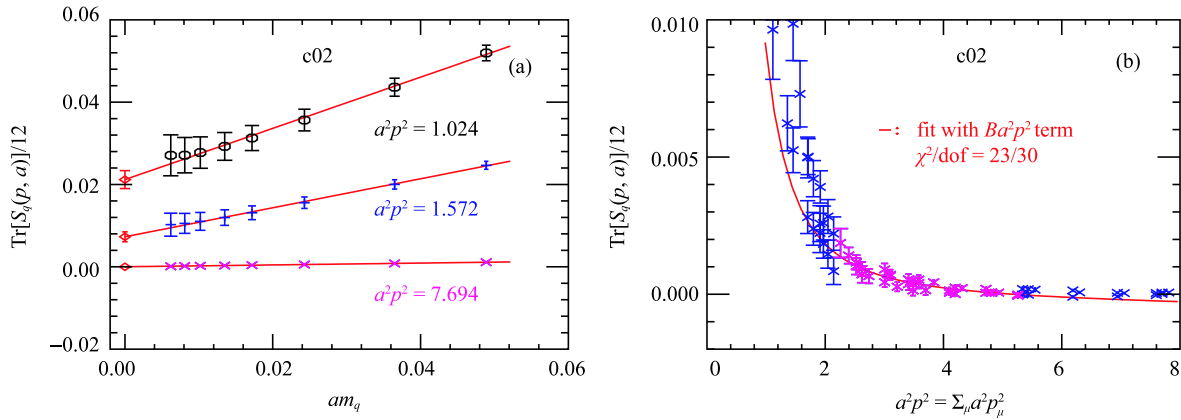

Fig. 6.   (color online) (a) Examples of linear extrapolation of the scalar form factor to the quark massless limit at three typical momentum values. (b) Fitting of the scalar form factor in the chiral limit to Eq. (17) on ensemble c02. The data points in purple ($a^2 p^2 \in [2.2, 5.3]$) are included in the fitting.

The results of $\langle\bar{\psi}\psi\rangle$ from the three ensembles are given in Tables 10 and 11. Table 10 is for fittings with a different p^2 window on each ensemble and Table 11 for fittings with the same p^2 window on all three ensembles. They are in agreement within errors.

Table 10. $\langle\bar{\psi}\psi\rangle^{\overline{\rm MS}}$(2 GeV) on the three ensembles from the analysis of the scalar form factor. The first uncertainty is statistical. The second is from the uncertainty of the lattice spacing. The third is an estimate of the truncation effects in the evaluations of the Wilson coefficients and α_s.

ensemble	$a^2p^2 \in$	$p^2 \in$/GeV^2	χ^2/dof	$(\langle\bar{\psi}\psi\rangle)^{1/3}$/MeV
c02	$[2.2, 5.3]$	$[6.7, 16.2]$	0.76	$-272(32)(6)(7)$
c01	$[1.8, 3.8]$	$[5.5, 11.6]$	1.02	$-278(35)(6)(9)$
c005	$[1.4, 3.1]$	$[4.3, 9.5]$	1.03	$-288(10)(7)(11)$

Table 11. $\langle\bar{\psi}\psi\rangle^{\overline{\rm MS}}$(2 GeV) from fittings of the scalar form factor in the same fitting window $a^2p^2 \in [2.0, 3.2]$ on all three ensembles. The three uncertainties are as explained in Table 10.

ensemble	χ^2/dof	$(\langle\bar{\psi}\psi\rangle)^{1/3}$/MeV
c02	1.00	$-299(35)(7)(9)$
c01	0.83	$-262(47)(6)(9)$
c005	0.86	$-280(16)(6)(9)$

The light sea quark mass dependence of $\langle\bar{\psi}\psi\rangle$ is again small compared with our uncertainties. Thus we do a constant fit similar to Fig. 4 in Section 4.1. What we obtain is

$$\langle\bar{\psi}\psi\rangle^{\overline{\rm MS}}(2\ {\rm GeV}) = (-284(13)\ {\rm MeV})^3$$
$$\text{(different fitting ranges)}, \qquad (18)$$

and

$$\langle\bar{\psi}\psi\rangle^{\overline{\rm MS}}(2\ {\rm GeV}) = (-282(16)\ {\rm MeV})^3$$
$$\text{(same fitting range)}. \qquad (19)$$

5   Summary

We determine the quark chiral condensate by fitting lattice data of the overlap quark propagator to its operator product expansion in the $\overline{\rm MS}$ scheme in Landau gauge. We perform two analyses. One uses the ratio of scalar to vector form factor of the propagator, which is supposed to have modest $\mathcal{O}(a^2g^2)$ lattice artifacts. The other one uses the scalar form factor. We use the result from the second analysis to estimate the uncertainty

from the $\mathcal{O}(a^2g^2)$ artifacts. The fitting range of the momentum in our analyses is varied to check the stability of the results. The truncation errors in evaluating the Wilson coefficients and α_s are also examined. Three ensembles of 2+1-flavor domain wall fermion configurations are used to check the light sea quark mass dependence.

We take the number in Eq. (14) as our final result. The difference between the center values in Eq. (14) and Eq. (18) is taken as a systematic uncertainty due to the $\mathcal{O}(a^2g^2)$ effects in our data. That is to say, our final result is

$$\langle\bar{\psi}\psi\rangle^{\overline{\rm MS}}(2\ {\rm GeV}) = (-304(15)(20)\ {\rm MeV})^3. \qquad (20)$$

Here the first error contains uncertainties from statistics, the lattice spacing and truncations in perturbative calculations of the Wilson coefficients and α_s.

Our result, Eq. (20), with a relatively large error bar, agrees with the FLAG-3 average $\Sigma^{1/3} = 274(3)$ MeV [10] for $N_{\rm f} = 2+1$ flavor lattice calculations. The RBC-UKQCD Collaborations found a lower center value $\Sigma^{1/3} = 256(6)$ MeV for the condensate in [18]. They used domain wall valence quarks on the same ensembles (c005 and c01) as used in this work and three more ensembles with a finer lattice spacing. A combined continuum and chiral extrapolation of pseudoscalar meson masses and decay constants was performed with finite volume next-to-leading order $SU(2)$ chiral perturbation theory or a simple analytic ansatz. The condensate as well as other low energy constants was obtained. Our result, obtained at one lattice spacing, agrees with their number within 2σ. In an updated analysis [1] by the RBC-UKQCD Collaborations more ensembles are used, including those with nearly physical pion masses. A larger center value $\Sigma^{1/3} = 275.9(1.9)(1.0)$ MeV was obtained for the chiral condensate, which is included in the FLAG-3 average [10].

To improve our work, the $\mathcal{O}(a^2g^2)$ effects should be calculated and removed from the lattice data of the quark propagator. With more statistics the effects of the $\langle A^2\rangle$ term can be checked carefully. Furthermore, calculations at more lattice spacings should be done to enable a continuum extrapolation.

References

1　T. Blum et al (RBC and UKQCD Collaborations), Phys. Rev. D, **93**(7): 074505 (2016) doi:10.1103/PhysRevD.93.074505 [arXiv:1411.7017 [hep-lat]]

2　A. Bazavov et al, PoS LATTICE, **2010**: 083 (2010) [arXiv:1011.1792 [hep-lat]]

3　K. Cichy, E. Garcia-Ramos, and K. Jansen, JHEP, **1310**: 175 (2013) doi:10.1007/JHEP10(2013)175 [arXiv:1303.1954 [hep-lat]]

4　S. Borsanyi, S. Durr, Z. Fodor, S. Krieg, A. Schafer, E. E. Scholz, and K. K. Szabo, Phys. Rev. D, **88**: 014513 (2013) doi:10.1103/PhysRevD.88.014513 [arXiv:1205.0788 [hep-lat]]

5　S. D rr et al (Budapest-Marseille-Wuppertal Collaboration), Phys. Rev. D, **90** (11): 114504 (2014) doi:10.1103/ PhysRevD.90.114504 [arXiv:1310.3626 [hep-lat]]

6　R. Baron et al (ETM Collaboration), JHEP, **1008**: 097 (2010) doi:10.1007/JHEP08(2010)097 [arXiv:0911.5061 [hep-lat]]

7　B. B. Brandt, A. Jttner, and H. Wittig, JHEP, **1311**: 034 (2013) doi:10.1007/JHEP11(2013)034 [arXiv:1306.2916 [hep-lat]]

8　G. P. Engel, L. Giusti, S. Lottini, and R. Sommer, Phys. Rev. D, **91** (5): 054505 (2015) doi:10.1103/PhysRevD.91.054505 [arXiv:1411.6386 [hep-lat]]

9　T. DeGrand, Z. Liu, and S. Schaefer, Phys. Rev. D, **74**: 094504 (2006); Phys. Rev. D, **74**: 099904 (2006) doi:10.1103/ PhysRevD.74.094504, 10.1103/PhysRevD.74.099904 [hep-lat/0608019]

10　S. Aoki et al, arXiv:1607.00299 [hep-lat]

11　F. Burger, V. Lubicz, M. M ller-Preussker, S. Simula, and C. Urbach, Phys. Rev. D, **87** (3): 034514 (2013); Phys. Rev. D, **87**: 079904 (2013) doi:10.1103/PhysRevD.87.034514, 10.1103/PhysRevD.87.079904 [arXiv:1210.0838 [hep-lat]]

12　P. O. Bowman, U. M. Heller, D. B. Leinweber, M. B. Parappilly, and A. G. Williams, Nucl. Phys. Proc. Suppl., **161**: 27 (2006) doi:10.1016/j.nuclphysbps.2006.08.078

13　D. Becirevic and V. Lubicz, Phys. Lett. B, **600**: 83 (2004) doi:10.1016/j.physletb.2004.07.065 [hep-ph/0403044]

14　P. Boucaud, J. P. Leroy, A. L. Yaouanc, J. Micheli, O. Pene, and J. Rodriguez-Quintero, Phys. Rev. D, **81**: 094504 (2010) doi:10.1103/PhysRevD.81.094504 [arXiv:0912.3173 [hep-lat]]

15　V. Gimenez, V. Lubicz, F. Mescia, V. Porretti, and J. Reyes, Eur. Phys. J. C, **41**: 535 (2005) doi:10.1140/epjc/s2005-02250-9 [hep-lat/0503001]

16　K. G. Chetyrkin and A. Maier, JHEP, **1001**: 092 (2010) doi:10.1007/JHEP01(2010)092 [arXiv:0911.0594 [hep-ph]]

17　K. G. Chetyrkin and A. Retey, Nucl. Phys. B, **583**: 3 (2000) doi:10.1016/S0550-3213(00)00331-X [hep-ph/9910332]

18　Y. Aoki et al (RBC and UKQCD Collaborations), Phys. Rev. D, **83**: 074508 (2011) [arXiv:1011.0892 [hep-lat]]

19　Y. B. Yang et al, Phys. Rev. D, **92** (3): 034517 (2015) [arXiv:1410.3343 [hep-lat]]

20　H. Neuberger, Phys. Lett. B, **417**: 141 (1998) [hep-lat/9707022]

21　T. -W. Chiu and S. V. Zenkin, Phys. Rev. D, **59**: 074501 (1999) [hep-lat/9806019]

22　Z. Liu et al (chiQCD Collaboration), Phys. Rev. D, **90** (3): 034505 (2014) [arXiv:1312.7628 [hep-lat]]

23　Y. Bi, H. Cai, Y. Chen, M. Gong, Z. Liu, H. X. Qiao, and Y. B. Yang, Chin. Phys. C, **40** (7): 073106 (2016) doi:10.1088/1674-1137/40/7/073106 [arXiv:1510.07354 [hep-ph]]

24　B. Blossier et al, Phys. Rev. D, **83**: 074506 (2011) doi:10.1103/ PhysRevD.83.074506 [arXiv:1011.2414 [hep-ph]]

25　B. Blossier et al (ETM Collaboration), Phys. Rev. D, **82**: 034510 (2010) doi:10.1103/PhysRevD.82.034510 [arXiv:1005.5290 [hep-lat]]

26　C. Patrignani et al (Particle Data Group Collaboration), Chin. Phys. C, **40** (10): 100001 (2016). doi:10.1088/1674-1137/40/10/100001

27　G. Martinelli, C. Pittori, C. T. Sachrajda, M. Testa, and A. Vladikas, Nucl. Phys. B, **445**: 81 (1995) [arXiv:hep-lat/9411010]